JOURNAL OF MATERIALS SCIENCE 31 (1996) 157–163

Liquid phase behaviour in nonstoichiometric calcium-doped lanthanum chromites*

J. D. CARTER‡, M. M. NASRALLAH, H. U. ANDERSON
Department of Ceramic Engineering, University of Missouri-Rolla, Rolla, MO 65401, USA

The sinterability of $(La,Ca)CrO_3$ is analysed by comparing the liquid phase behaviour in A-site excess and A-site deficient compositions (referring to the ABO_3 formula). The analysis shows that a series of A-site excess and deficient compositions form distinct liquid phases belonging to the $CaO–Cr_2O_3$ phase system. Although both series experience grain growth and densification due to the presence of a liquid phase, the A-site excess compositions exhibit greater shrinkage and sinter to closed porosity, whereas the A-site deficient compositions remain porous. During the final stages of sintering, surplus liquid from the A-site excess material exudes to the free-surface forming a layer of uniform thickness. By comparison, the liquid in the A-site deficient composition segregates to the free-surface forming islands and leaving porous regions in the bulk matrix. It is concluded that the different liquid phase compositions in the A-site excess and A-site deficient $(La,Ca)CrO_3$ have dissimilar wetting characteristics during the later stages of sintering. The A-site deficient liquid forms a premature solid phase, which accounts for the difference in sintering behaviour.

1. Introduction

Lanthanum chromite has many of the desired properties for an interconnect in the solid oxide fuel cell (SOFC). When doped with Ca, it has an electrical conductivity in air up to 60 $S\,cm^{-1}$ at 1000 °C [1], its thermal expansion coefficient can be matched with other SOFC components [2] and it is thermodynamically stable in both reducing and oxidizing environments [3].

The monolithic SOFC design [4] requires the co-sintering of all cell components. This process must proceed in air, at temperatures or below 1400 °C to reduce interaction between cell components, and retain open porosity in the anode and cathode. After sintering, the electrolyte and the interconnect must be impermeable to oxidizing and fuel gases.

Several studies have been directed towards developing an air sintering process at temperatures less than 1400 °C. In $(La,Ca)CrO_3$, a liquid phase is formed which can be used to aid sintering. This liquid is related to the $CaO–Cr_2O_3$ phase system [5]. For this liquid phase to be effective, an excess amount of La and Ca is added to the system so that $(La + Ca)/Cr > 1$ [6, 7]. This results in nonstoichiometric compositions which are commonly referred to as "B-site deficient" or "A-site excess".

Sakai *et al.* [16] have characterized the liquid phase in A-site excess $(La,Ca)CrO_3$. They describe it as an oxychromate liquid belonging to the $CaO–Cr_2O_3$ pseudobinary system. The exsolved second phase in $(La,Ca)CrO_3$ is identified by the general formula $Ca_m(CrO_4)_n$. (This notation will also be adopted in the present work, referring to both Ca excess and deficient compositions). They also observed that $Ca_m(CrO_4)_n$ changes composition during sintering. Initially, $Ca_5(CrO_4)_3OH$ formed on free-surfaces after sintering at 1300 °C; but after sintering at 1500 °C, CaO was detected at the triple points of the grains.

Chick and co-workers [5, 7] compared the differences in sintering A-site excess and A-site deficient $(La,Ca)CrO_3$ and $(Y,Ca)CrO_3$. The La and Y chromites were reported to exhibit similar sintering behaviour. Phase analysis of $(La,Ca)CrO_3$ suggested that $Ca_m(CrO_4)_n$ had a different composition for A-site excess and A-site deficient specimens. A dilatometry study showed that in the later stages of sintering, the shrinkage in A-site excess compositions was ten times greater than that of the A-site deficient material. Chick and co-workers concluded that the difference in sinterability between A-site excess and A-site deficient $(La,Ca)\ CrO_3$ was due to the ineffectiveness of the A-site deficient liquid towards densification.

The present investigation sought to further the characterization of $Ca_m(CrO_4)_n$ in the $(La,Ca)CrO_3$ system. A-site excess and A-site deficient materials are compared through the use of scanning electron

*Based on a dissertation submitted by J. David Carter for the PhD degree in Ceramic Engineering at the University of Missouri-Rolla, Rolla MO, 1992. Support was granted by Argonne National Laboratory and Department of Energy.
‡Present address: Chemical Technology Division, Argonne National Laboratory, 9700 South Cass Avc., Argonne, Illinois 60439-4837, USA.

microscopy (SEM), energy dispersive spectrometry (EDS), X-ray powder diffraction (XRD), and differential thermal analysis (DTA). The wetting behaviour of $Ca_m(CrO_4)_n$ during sintering is shown to vary according to the (La + Ca)/Cr ratio. This behaviour and premature solid formation are found to be critical factors in determining the sinterability of (La,Ca)CrO_3.

2. Experimental procedure

Powder specimens were prepared having the precursor compositions: $(La_{0.6}Ca_{0.4})_xCrO_4$, where $x = 0.95, 0.98, 0.99, 1.00, 1.01, 1.02$ and 1.05. A large amount of Ca (~40 at %) was added into the system so that $Ca_m(CrO_4)_n$ could be easily observed and analysed. Samples were synthesized and processed in the low temperature monazite-type form to control the distribution of secondary phases. Above 700 °C, (La,Ca)CrO_4 transforms into $LaCrO_3$, $CaCrO_4$ and other unidentified minor phases which, at higher temperatures form a (La,Ca)CrO_3 solid solution and a $Ca_m(CrO_4)_n$ liquid phase [8]. The present work is concerned mainly with the perovskite phase, so the general form, (La,Ca)CrO_3 will be written when referring to compositions which have been heated above the $LaCrO_4$ to $LaCrO_3$ transformation temperature.

Powder synthesis was performed using a modified liquid mix process [9]. The raw materials, $La_2(CO_3)_3$, $CaCO_3$, and a $Cr(NO_3)_3$ solution, (nominal purities 99%) were mixed in a Pyrex beaker with distilled water and nitric acid and heated on a hot plate to dissolve the solids. Citric acid (CA) and ethylene glycol (EG) were then added to the solution so that CA/EG/metal oxide = 1:1:1 molar ratio. Heating of the mixture was continued to remove water until the viscosity had noticeably increased. The viscous solution was then placed in a drying oven at 120 °C. At this point, the solution ignited and charred. The char was milled in reagent ethyl alcohol for eight hours to reduce the agglomeration inherent to the process. Calcination took place under flowing argon for 8 h at 550 °C. Phase analysis was made by XRD (Model 2000, Scintag Inc., Santa Clara, CA).

The calcined powders were uniaxially pressed into 12.7 mm diameter × 3.2 mm thick discs at 500 MPa. Bulk green and sintered densities were determined using both dimensional measurements and the Archimedes' method. The discs were heated at a rate of 5 °C min^{-1} and sintered at 1300–1450 °C for 2–100 h.

Several specimens having the compositions: $(La_{0.6}Ca_{0.4})_{0.99}CrO_3$, and $(La_{0.6}Ca_{0.4})_{1.02}CrO_3$ were air quenched to room temperature from various temperatures during a sintering run. The furnace heating rate was 4 °C min^{-1}, and isothermal holds were made at 1030 °C for 2 h and at 1350 °C for 2 h. Microanalysis on quenched and sintered samples was performed by SEM and EDS (Model T33A, Jeol USA, Peabody, MA/Kevex Instruments, Valencia, CA).

The melting characteristics of the liquid phase in $(La_{0.6}Ca_{0.4})_{0.99}CrO_3$ and $(La_{0.6}Ca_{0.4})_{1.02}CrO_3$ were compared with $CaCrO_4$ by using DTA (STA Model 409, Netzsch Inc., Exton, PA).

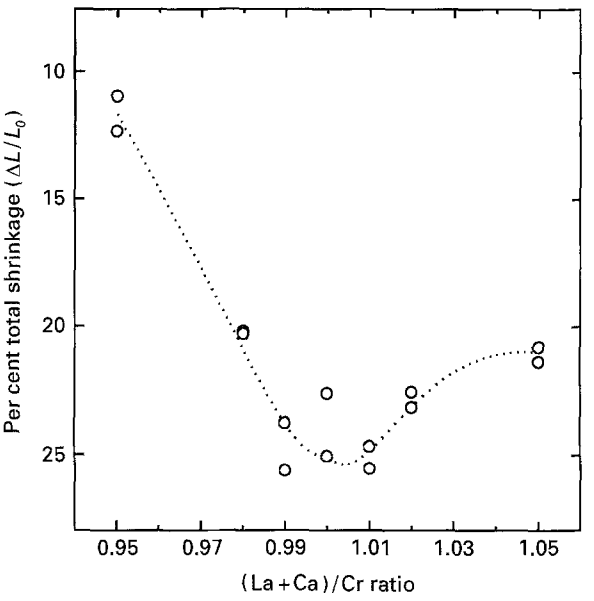

Figure 1 Per cent total shrinkage versus (La + Ca)/Cr cation ratio of $(La_{0.6}Ca_{0.4})_xCrO_3$. Sintered 1400 °C for 2 h.

3. Results

3.1. Porosity and shrinkage

The sintering behaviour of $(La_{0.6}Ca_{0.4})_xCrO_3$ compositions were studied by measuring shrinkage, density and the porosity of specimens sintered under various temperatures and time periods. A plot of shrinkage with respect to the (La + Ca)/Cr cation ratio under the sintering conditions of 1400 °C/2 h provides an indication of sinterability. In Fig. 1, the total shrinkage increases rapidly as (La + Ca)/Cr increases from 0.95 to 0.99. Maximum shrinkage is obtained when the cation ratio is between 0.99 and 1.01.

Density measurements were difficult to correlate, because the amount of exsolved $Ca_m(CrO_4)_n$ changed throughout the process, making the theoretical density difficult to track. However, a comparison of the apparent density (solids + closed porosity) with bulk density (solids + total porosity) yields open porosity, which does provide a good indication of sinterability. Fig. 2 is a plot of the per cent open porosity versus the (La + Ca)/Cr cation ratio for $(La_{0.6}Ca_{0.4})_xCrO_3$ where x ranges from 0.95 to 1.05, sintered at 1400 °C for 2 h. The open porosity decreases as (La + Ca)/Cr increases from 0.95 to 1.0. Between 1.0 and 1.05, it approaches zero.

3.2. Sintering behaviour

Evidence of the liquid phase was readily observed in quenched specimens. Fig. 3 is a SEM image showing the recrystallized liquid as a dark glass-like mass enveloping the lighter (La,Ca)CrO_3 particles. Similar microstructures were common in all of the $(La_{0.6}Ca_{0.4})_xCrO_3$ compositions under similar conditions. According to EDS, the bulk quenched liquid is composed of Ca, Cr and O. X-ray analysis confirmed the presence of mainly $CaCrO_4$ and sometimes other $Ca_m(CrO_4)_n$ phases in sintered specimens.

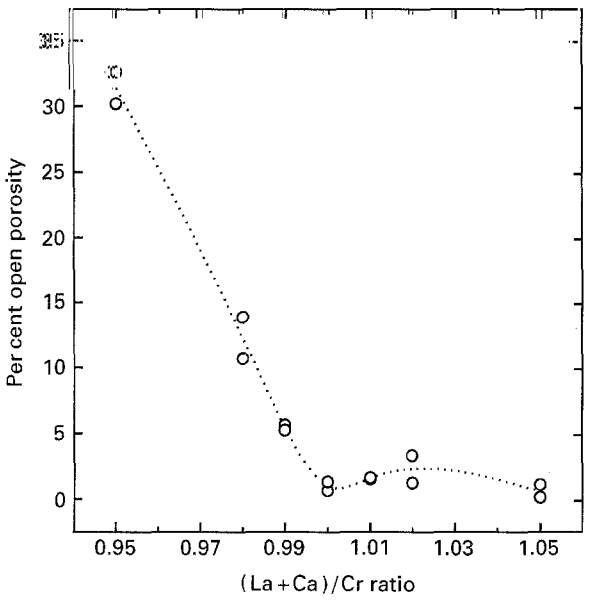

Figure 2 Per cent open porosity versus (La + Ca)/Cr cation ratio for $(La_{0.6}Ca_{0.4})_xCrO_3$. Sintered 1400 °C for 2 h.

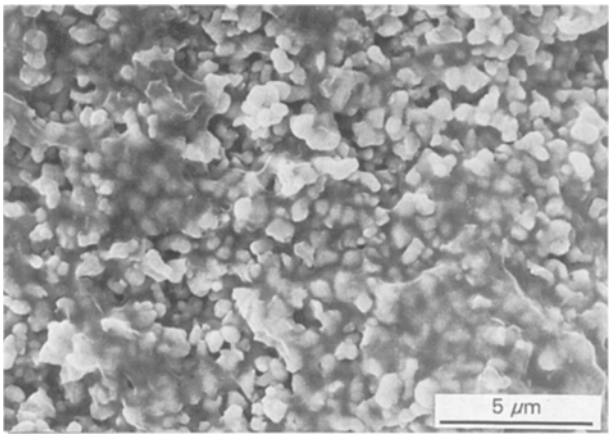

Figure 3 A SEM image of a polished surface of $(La_{0.6}Ca_{0.4})_{0.95}CrO_3$. Sintered 1300 °C for 2 h.

The sintering of $(La_{0.6}Ca_{0.4})_{0.99}CrO_3$ and $(La_{0.6}Ca_{0.4})_{1.02}CrO_3$ were compared by SEM analysis on a series of quenched samples. Figs 4 through to 6 show the behaviour of the two compositions. Each specimen pair were air quenched from similar temperatures during the sintering process. The micrographs represent the fracture surface of the specimens.

Fig. 7 is a cross-section of $(La_{0.6}Ca_{0.4})_{1.02}CrO_3$, showing a dark layer which has formed on the free-surface. The liquid has spread into a uniform layer along the free-surface after being squeezed out of the grain boundaries as the grains coalesced. The surface layer was identified by XRD and found to be $Ca_5(CrO_4)_3OH$.

Fig. 8a shows a back-scatter image of the cross-section of $Ca_m(CrO_4)_n$ crystals on the surface of $(La_{0.6}Ca_{0.4})_{0.99}CrO_3$ and Fig. 8b is the top view of a polished specimen. Surrounding this mass is a large porous region with a radius of 100 μm or more. Energy dispersive analysis indicated that these crystals are Ca-poor, although XRD only showed the presence of $CaCrO_4$.

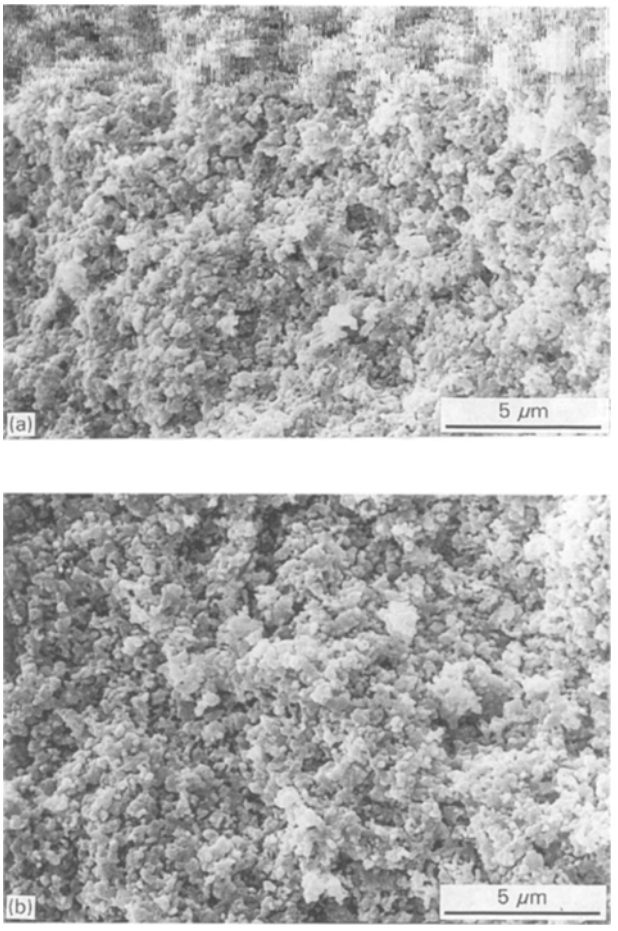

Figure 4 SEM images of fracture surfaces of (a) $(La_{0.6}Ca_{0.4})_{0.99}CrO_3$ and (b) $(La_{0.6}Ca_{0.4})_{1.02}CrO_3$ heated to 740 °C and air quenched to room temperature.

Annealing experiments demonstrated the difficulty in dissolving large amounts of Ca into $(La,Ca)CrO_3$. Specimens containing 40 at % Ca with (La + Ca)/Cr cation ratios of 0.95 to 1.05 contained residual recrystallized liquid in the grain boundaries after long term annealing. For example, Fig. 9 is a back-scatter image of $(La_{0.6}Ca_{0.4})_{1.05}CrO_3$ sintered and annealed at 1300 °C for 100 h. According to EDS, the dark cubic phase contains Ca and O.

3.3. Melting behaviour

The characteristics of liquid formation with respect to stoichiometry, are further illustrated by comparing the DTA curves of $CaCrO_4$, $(La_{0.6}Ca_{0.4})_{1.02}CrO_3$ and $(La_{0.6}Ca_{0.4})_{0.99}CrO_3$, as shown in Fig. 10. In the upper set of curves, the onset of melting takes place at nearly the same temperature for each composition. In particular, the $CaCrO_4$ and $(La_{0.6}Ca_{0.4})_{0.99}CrO_3$ curves display a similar, single step melting process. The double peaks corresponding to $(La_{0.6}Ca_{0.4})_{1.02}CrO_3$, indicate that the associated phase melts in two stages.

The crystallization peaks in the lower section occur at lower temperatures which reflects supercooling of the liquid. The $CaCrO_4$ composition crystallizes first, and the other two liquids crystallize about 10 °C

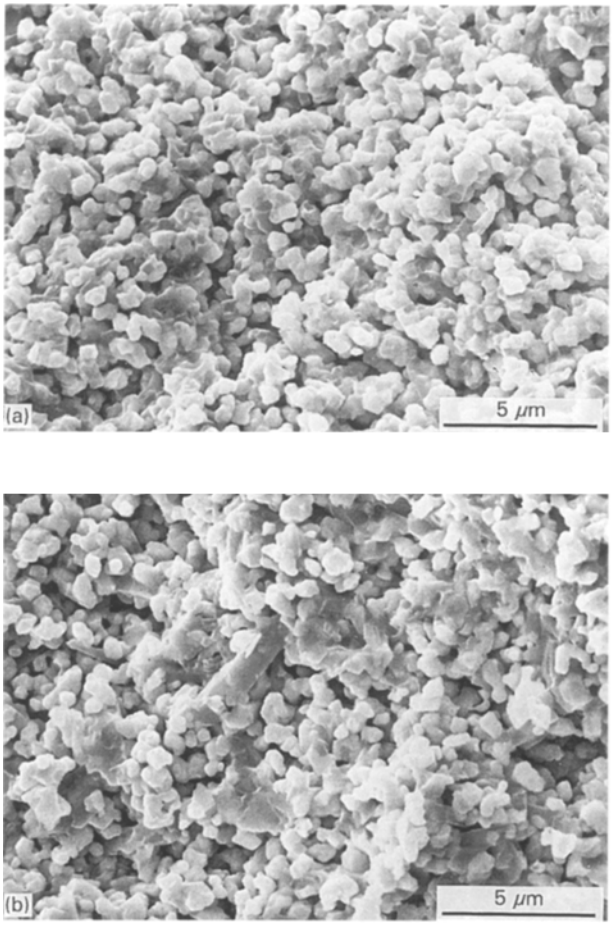

Figure 5 SEM images of fracture surfaces of (a) $(La_{0.6}Ca_{0.4})_{0.99}CrO_3$ and (b) $(La_{0.6}Ca_{0.4})_{1.02}CrO_3$ heated to 1030 °C and air quenched to room temperature.

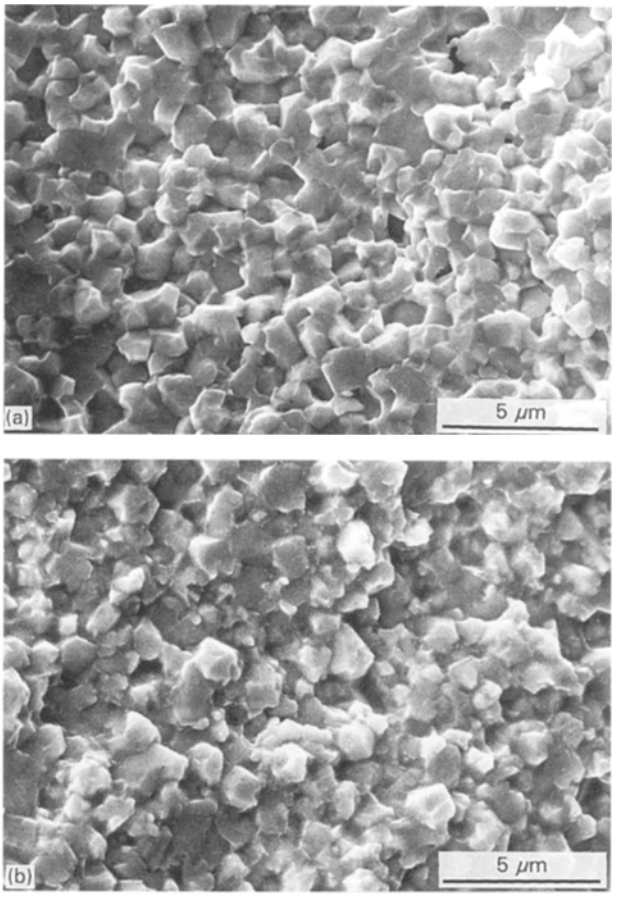

Figure 6 SEM images of fracture surfaces of (a) $(La_{0.6}Ca_{0.4})_{0.99}CrO_3$ and (b) $(La_{0.6}Ca_{0.4})_{1.02}CrO_3$ heated to 1350 °C for 2 h and air quenched to room temperature.

lower. The liquid in $(La_{0.6}Ca_{0.4})_{1.02}CrO_3$ again shows a double peak which suggests a two step crystallization process.

4. Discussion

The large amount of exsolved $Ca_m(CrO_4)_n$ in the system, made it difficult to correlate the sinterability of $(La_{0.6}Ca_{0.4})_xCrO_3$ compositions directly by shrinkage or density measurements (Fig. 1). For example, $(La_{0.6}Ca_{0.4})_{0.99}CrO_3$ had a shrinkage comparable to $(La_{0.6}Ca_{0.4})_{1.01}CrO_3$, which seems to contradict the results of Sakai *et al.* [6] and Chick *et al.* [7]. Possibly, enough liquid was present to overcome some of the effects of stoichiometry. Obviously, the amount of total Ca added to these compositions exceeded optimized values and should be reduced if these compositions are to be used as an interconnect material in SOFC applications. This is evident from the annealing experiment (Fig. 9). A former study [10] has suggested that < 25 at % Ca in $(La,Ca)CrO_3$ approaches an optimal composition.

Notable differences in densification became evident from porosity measurements (Fig. 2). The A-site deficient compositions showed higher open porosity than their A-site excess counterparts.

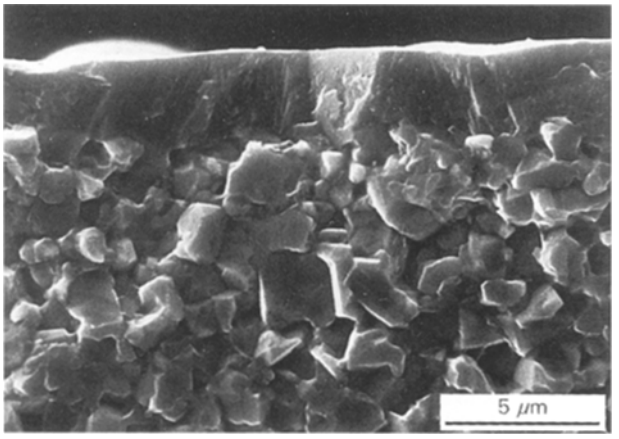

Figure 7 A SEM image of a fracture surface of $(La_{0.6}Ca_{0.4})_{1.02}CrO_3$ sintered at 1350 °C for 4 h.

Microscopic analysis of a series of quenched specimens provided a visual investigation of the sintering process. Initially, specimen pairs of A-site excess and deficient compositions followed the same general steps of densification. Both transformed to the perovskite structure below 740 °C as evidenced by XRD. Grain growth has occurred so that the primary particles can be resolved (Fig. 4a and b).

From previous work [8] it is known that $CaCrO_4$ loses oxygen and begins to form a solid solution with $LaCrO_3$. Excess Ca which is not incorporated in the

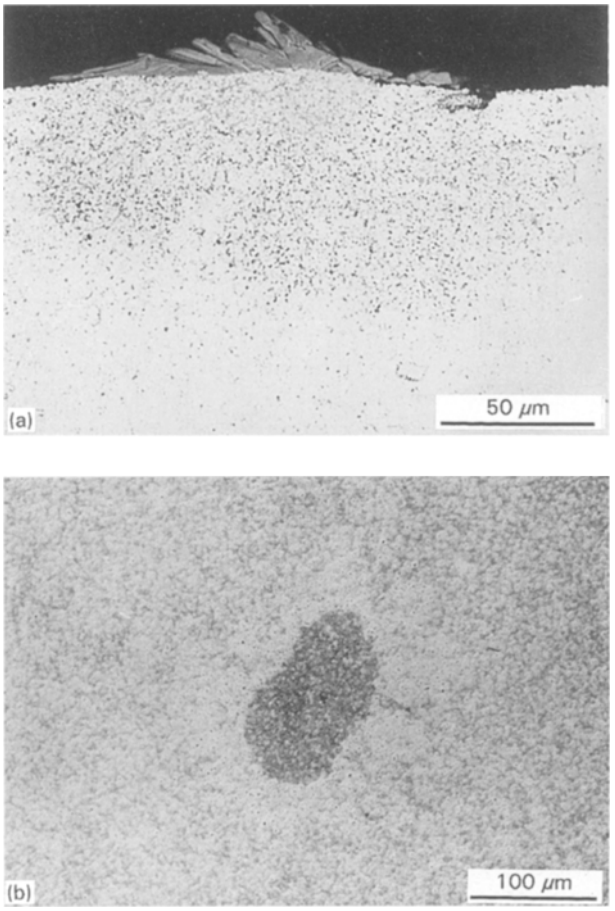

Figure 8 (a) A SEM back-scatter image of a fracture surface of $(La_{0.6}Ca_{0.4})_{0.99}CrO_3$ sintered at 1350 °C for 2 h. (b) Polished $(La_{0.6}Ca_{0.4})_{0.99}CrO_3$ sintered at 1400 °C for 2 h.

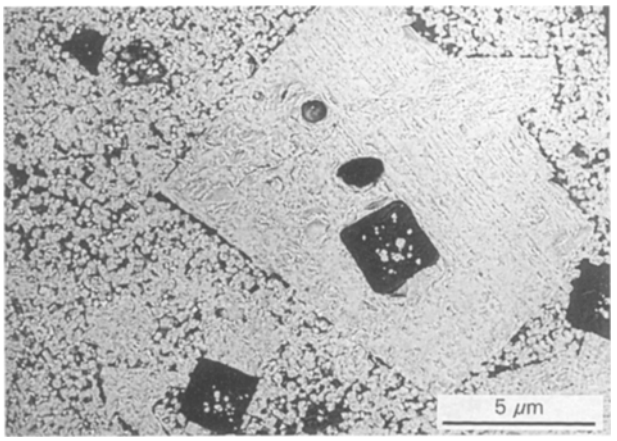

Figure 9 A SEM back-scatter image of polished $(La_{0.6}Ca_{0.4})_{1.05}CrO_3$ sintered at 1300 °C for 100 h.

solid solution segregates along with Cr and O to the free-surface in both the A-site excess and A-site deficient materials (Figs 7 and 8).

Upon melting $Ca_m(CrO_4)_n$, all compositions experienced rapid grain growth (Fig. 5a and b). The recrystallized liquid is identified in either figure as darker, irregular masses; the lighter equiaxed grains are $(La,Ca)CrO_3$. It appears that $Ca_m(CrO_4)_n$ segregates from $(La,Ca)CrO_3$. Continued heating was accompanied with further grain growth and the spreading of liquid (Fig. 3). Fig. 6 is a comparison of the two compositions after a two hour hold at 1350 °C.

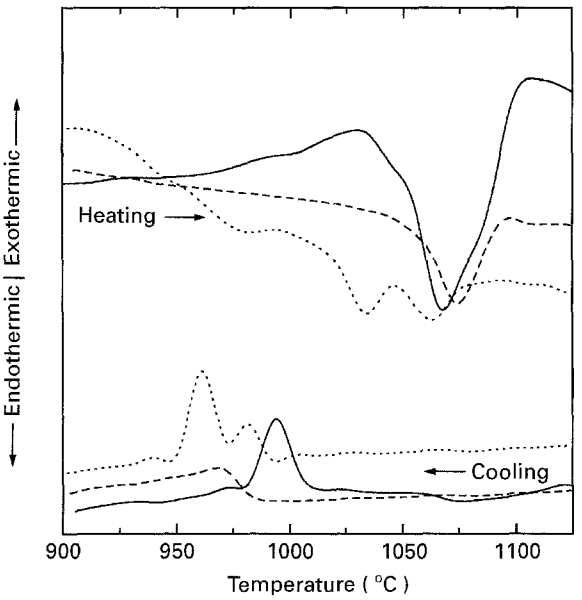

Figure 10 A DTA comparison of the melting and freezing peaks in $CaCrO_4$, $(La_{0.6}Ca_{0.4})_{1.02}CrO_3$, and $(La_{0.6}Ca_{0.4})_{0.99}CrO_3$ powders. Heating rate, 10 °C min^{-1}.— $CaCrO_4$, ---- $(La_{0.6}Ca_{0.4})_{1.02}CrO_3$ and ——— $(La_{0.6}Ca_{0.4})_{0.99}CrO_3$.

From this series of micrographs, the sinterability of the two compositions appear to be quite similar. In both cases a liquid phase forms and spreads, grain growth occurs at similar rates and the final grain sizes are comparable. This did not allow any explanation of the observed differences in shrinkage and porosity. However, differences become apparent by examination of the specimen free-surfaces.

A comparison of Figs 7 and 8 illustrates the difference between the liquid phases in the final sintering stages of A-site excess and A-site deficient compositions. The liquid on the free-surface of the A-site excess specimen (Fig. 7) has spread into a uniform 3 μm layer, demonstrating good wetting and spreading characteristics. This is desirable for optimum liquid phase sintering. In contrast, the $Ca_m(CrO_4)_n$ phase in the A-site deficient material (Fig. 8) formed a 100 μm diameter island on the surface. The large volume of porosity surrounding this island is a result of the segregation of the $Ca_m(CrO_4)_n$ liquid from the $(La,Ca)CrO_3$ matrix. This $Ca_m(CrO_4)_n$ phase appears to be more crystalline and it is believed that it contained Ca–Cr–O solids throughout sintering, because $CaCr_2O_4$ whiskers were observed to grow from some of the A-site deficient compositions while at the sintering temperature.

The divergent behaviour of the $Ca_m(CrO_4)_n$ compositions towards densification may be understood by reference to the $CaO–Cr_2O_3$ phase diagram. Fig. 11 is a pseudobinary phase diagram of the $CaO–Cr_2O_3$ system after the combined work of Kaiser *et al.* [11] and Pánek [12]. Kaiser *et al.* and others [13] studied compositions in the Ca-rich region of the diagram, whereas Pánek appears to have worked more in the Ca-poor region.

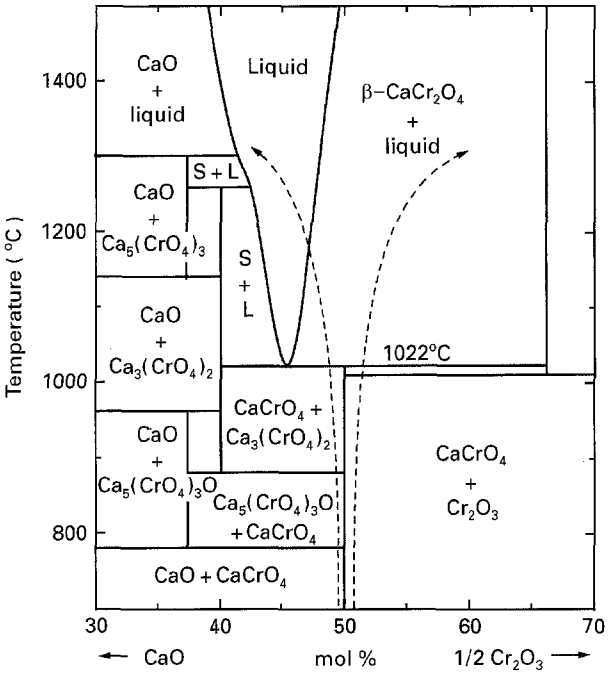

Figure 11 The $CaO-Cr_2O_3$ pseudobinary phase diagram after Kaiser *et al.* [11] and Pánek [12].

Assuming that $(La,Ca)CrO_3$ retains its stoichiometry with respect to the A and B cations, i.e. $(La + Ca)/Cr \equiv 1$, any nonstoichiometry within a given system is presumed to appear in the secondary phases. Therefore, when Ca dissolves into the (La,Ca) CrO_3 matrix, it is accompanied with stoichiometric amounts of Cr and O. This process of dissolution consequently induces a change in the composition of the $Ca_m(CrO_4)_n$ phase in nonstoichiometric systems.

The change in composition of $Ca_m(CrO_4)_n$, while heating is illustrated by the dashed arrows in Fig. 11. The lines are estimated and their curvature depend on the kinetics of dissolution of $CaCrO_4$ into $(La,Ca)CrO_3$. The initial composition of $Ca_m(CrO_4)_n$ at low temperature depends on the A/B stoichiometry and the amount of exsolved $CaCrO_4$. A different A/B ratio in $(La,Ca)CrO_3$ or mole fraction of exsolved $CaCrO_4$ will shift the initial composition of the secondary phase along the composition axis. For example, if $(La,Ca)CrO_3$ was initially prepared as A-site excess, and no $CaCrO_4$ was exsolved, the secondary phase would be CaO.

Upon heating A-site excess $(La,Ca)CrO_3$, the initial composition of the exsolved phase starts to the left of the $CaCrO_4$ composition line. As the temperature is increased the Ca solubility also increases and Ca, Cr and O begin to dissolve into the perovskite matrix. The Ca content of $Ca_m(CrO_4)_n$ will increase towards the CaO end member. At 1022 °C, a liquid phase forms with some amount of solid β-$CaCr_2O_4$. As heating continues, the liquid composition changes towards CaO and the solid β-$CaCr_2O_4$ disappears. At some point the melt becomes 100% liquid. The above SEM study (Fig. 7) showed that good wetting and spreading behaviour attend this liquid phase system throughout the sintering process.

In A-site deficient $(La,Ca)CrO_3$, the Ca content of $Ca_m(CrO_4)_n$ decreases towards the Cr_2O_3 end member with increasing temperature and Ca solubility. At some point, a solid network is formed between β-$CaCr_2O_4$ and $(La,Ca)CrO_3$ grains and densification by particle rearrangement stops. The remaining liquid eventually segregates from the matrix forming islands on the free-surface (Fig. 8). Regions surrounding these islands are characteristically porous.

Differential thermal analysis also indicated deviating behaviour in the opposing liquid phases. From Fig. 11, Ca-rich $Ca_m(CrO_4)_n$ should produce a DTA curve with two melting peaks, one near 1022 °C, the eutectic temperature, and one at a higher temperature upon complete melting of the liquid. Conversely, the DTA curve of Cr-rich $Ca_m(CrO_4)_n$ would contain only one broad peak, beginning at the eutectic temperature since there would be no other reaction expected. The experimental DTA curves of Fig. 10 follow this description.

5. Conclusions

The present study has examined the difference in densification between A-site excess and A-site deficient $(La,Ca)CrO_3$. A liquid phase forms in both stoichiometries which promotes grain growth and densification. However during the final stages of sintering, the behaviour of the excess and deficient systems diverge as a result of changes in composition of the respective liquids. The melt in the A-site excess material becomes 100% liquid and retains its wetting and spreading behaviour which is preferable for efficient densification. But the liquid in the A-site deficient material forms a solid which welds the $(La,Ca)CrO_3$ grains and then segregates to a free-surface, leaving a porous network of grains.

It is clear that the liquid phase composition has a pivotal effect on the sinterability of $(La,Ca)CrO_3$. Since the liquid phase composition is sensitive to the initial composition of $(La,Ca)CrO_3$, it would be profitable if $Ca_m(CrO_4)_n$ could be modified to accept composition changes near the Ca/Cr stoichiometric ratio and maintain the properties of a good sintering aid.

References

1. N. SAKAI, T. KAWADA, H. YOKOKAWA, M. DOKIYA and T. IWATA, *J. Mater. Sci.* **25** (1990) 4531.
2. N. SAKAI, T. KAWADA, H. YOKOKAWA, M. DOKIYA and T. IWATA, *Solid State Ionics* **40/41** (1990) 394.
3. R. BERJOAN, C. ROMAND and J.-P. COUTURES, *High Temp. Sci.* **13** (1980) 173.
4. D. C. FEE, R. K. STEUNENBERG, T. D. CLAAR, R. B. POEPPEL, J. P. ACKERMAN, in 1983 Fuel Cell Seminar (Courtesy Associates, Washington, D.C., 1983) p. 73.
5. L. A. CHICK, J. L. BATES and G. D. MAUPIN, in Proceedings of the Second International Symposium on Solid Oxide Fuel Cells, Athens Greece, July 1991, edited by F. Gross, P. Zegers, S. C. Singhal, O. Yamamoto. (Commission of the European Communities, Luxembourg, 1991) p. 621.
6. N. SAKAI, T. KAWADA, H. YOKOKAWA, M. DOKIYA and I. KOJIMA, *J. Amer. Ceram. Soc.* **76** (1993) 609.

7. L. A. CHICK, T. R. ARMSTRONG, D. E. McCREA – DY, G. W. COFFEY, G. D. MAUPIN and J. L. BATES, in Proceedings of the Third International Symposium on Solid Oxide Fuel Cells, Honolulu HI, 1993, Vol. 93–4, edited by S. C. Singhal, and H. Iwahara, (The Electrochemical Society, Inc., Pennington, NJ, 1993) p. 374.
8. J. D. CARTER, H. U. ANDERSON and M. G. SHUMSKY, *J. Mater. Sci.*, submitted.
9. L. TAI and P. LESSING, *J. Mater. Res.* **7** (1992) 511.
10. J. D. CARTER, V. SPRENKLE, M. M. NASRALLAH and H. U. ANDERSON, in Proceedings of the Third International Symposium on Solid Oxide Fuel Cells, Honolulu HI, 1993, Vol. 93–4, edited by S. C. Singhal, and H. Iwahara, (The Electrochemical Society, Inc., Pennington, NJ, 1993) p. 344.
11. A. KAISER, B. SOMMER and E. WOERMANN, *J. Amer. Ceram. Soc.* **75** (1992) 1463.
12. Z. PÁNEK, *Silikáty* **25** (1981) 169.
13. K. T. ADENDORFF, J. P. R. de VILLIERS and G. J. KRUGER, *J. Amer. Ceram. Soc.* **75** [6] (1992) 1416.

Received 18 July 1994
and accepted 17 July 1995